Purcell enhancement of fast-dephasing spontaneous emission from electron-hole droplets in high-Q silicon photonic crystal nanocavities

Hisashi Sumikura,* Eiichi Kuramochi, Hideaki Taniyama, and Masaya Notomi

NTT Nanophotonics Center, Nippon Telegraph and Telephone Corporation, 3-1 Morinosato Wakamiya, Atsugi, Kanagawa 243-0198, Japan and NTT Basic Research Laboratories, Nippon Telegraph and Telephone Corporation, 3-1 Morinosato Wakamiya, Atsugi, Kanagawa 243-0198, Japan

(Received 23 September 2016; revised manuscript received 7 November 2016; published 29 November 2016)

We have observed electron-hole droplet emission enhanced by silicon photonic crystal nanocavities with different Q values and simulated their Purcell effect using a semiclassical theory considering the temporal dephasing of the emission. When the photon loss rate of the nanocavities is smaller than the dephasing rate of the emission, the cavity-enhanced integrated photoluminescence (PL) intensity is unchanged by the cavity Q value. This is because the Purcell enhancement of the spontaneous emission rate is saturated in a high-Q region. In contrast, the peak intensity of the cavity-enhanced PL is proportional to the cavity Q value without saturation. These results suggest that a high-Q nanocavity is suitable for fabricating bright narrowband light emitting devices that concentrate the broadband emission energy of fast-dephasing emitters in a narrowband cavity resonance.

DOI: 10.1103/PhysRevB.94.195314

I. INTRODUCTION

Cavity-enhanced spontaneous emission (SE) has proved of great interest for fundamental and practical studies on cavity quantum electrodynamics and developments of energy-efficient and bright light emitting devices. This spontaneous emission enhancement, which is called the Purcell effect [1], results from the large local density of photon states artificially modified by photonic nanostructures. Photonic crystal (PhC) nanocavities and plasmonic nanostructures have been widely used to demonstrate the SE enhancement of light emitting materials [2,3]. Since the Purcell effect was first proposed in the 1940s, most experimental works assume that emitters do not have a homogeneous linewidth, which therefore excludes the pure dephasing of emitters. This assumption is acceptable for an optical cavity coupled with photon emitters that have a homogeneous linewidth narrower than the cavity linewidth, for example, alkali atoms, high-quality quantum dots (QDs), and impurity related emission centers in Si and diamond [4–7]. In the cases demonstrated so far, the Purcell effect predicts that the SE rate is proportional to the Q/V_c value of an optical cavity, where V_c is the mode volume. The high Q and small V_c are preferable features for the PhC nanocavities in terms of achieving a large SE enhancement.

In contrast, there are many photon emitters possessing a large emission dephasing rate. Emission dephasing is commonly fast for free excitons and electron-hole plasmas in semiconductors because of strong interactions with phonons, other electrons, and holes [8]. Thus far, theoretical studies discussed the Purcell effect for dephasing emitters with semiclassical and quantum mechanical approaches [9–13]. Furthermore, experimental works reported the Purcell effect on fast-dephasing emitters including bulk, quantum wells (QWs), and colloidal QDs of semiconductors [14–18]. However, we considered that several possible factors complicate the experimental results and analyses for the Purcell effect of fast-dephasing emitters. First, the free excitons and e-h plasmas are able to diffuse from small nanocavities. If there is no confinement mechanism, the diffusion can be counted as a nonradiative decay of the cavity-coupled emitters, which modifies an emission efficiency and time-resolved emission data. Second, most ensembles of emitters have a large inhomogeneity in the emission wavelength of each emitter. When a cavity enhances the emission from such emitters, the spectral and spatial hole burning induced by the cavity-enhanced SE should be taken into account [16] because of population redistributions of the cavity-coupled emitters. Finally, the cavity-Q dependences of the enhanced emission intensity and decay are necessary for proving the Purcell effect. All the above concerns should be resolved for a precise discussion on the emission dynamics of fast-dephasing excitons under the Purcell effect.

In this study, we observed the photoluminescence (PL) of electron-hole droplets (EHDs) from silicon PhC nanocavities with different cavity Q values in order to discuss the cavity-Q dependence of the SE enhancement while excluding diffusions and population redistributions of fast-dephasing emitters. We used PhC nanocavities with three missing air holes because we could vary their Q values by shifting the end holes of the cavities, which maintains its mode volume [19]. In general, it is also possible to vary their mode volumes by changing the entire cavity structure. However, in our experiment, only the Q value was carefully changed by a fine modification of the structure because a large structural change to vary the mode volume induces the large changes in the cavity Q value and nonradiative surface recombination simultaneously, which makes a large uncertainty when we compare the cavity-enhanced PL intensities and PL decay rates among different cavities.

In addition, an EHD is a suitable emitter with fast dephasing for two reasons. First, the outdiffusion of an EHD from a nanocavity is suppressed by its large mass thanks to the condensation of electron-hole (e-h) pairs [20]. This feature improves the electromagnetic coupling between the nanocavity and the emitters. Second, the spectral and spatial hole burning of the emitters induced by their cavity-enhanced SE is negligible when discussing the Purcell effect. The

*sumikura.hisashi@lab.ntt.co.jp

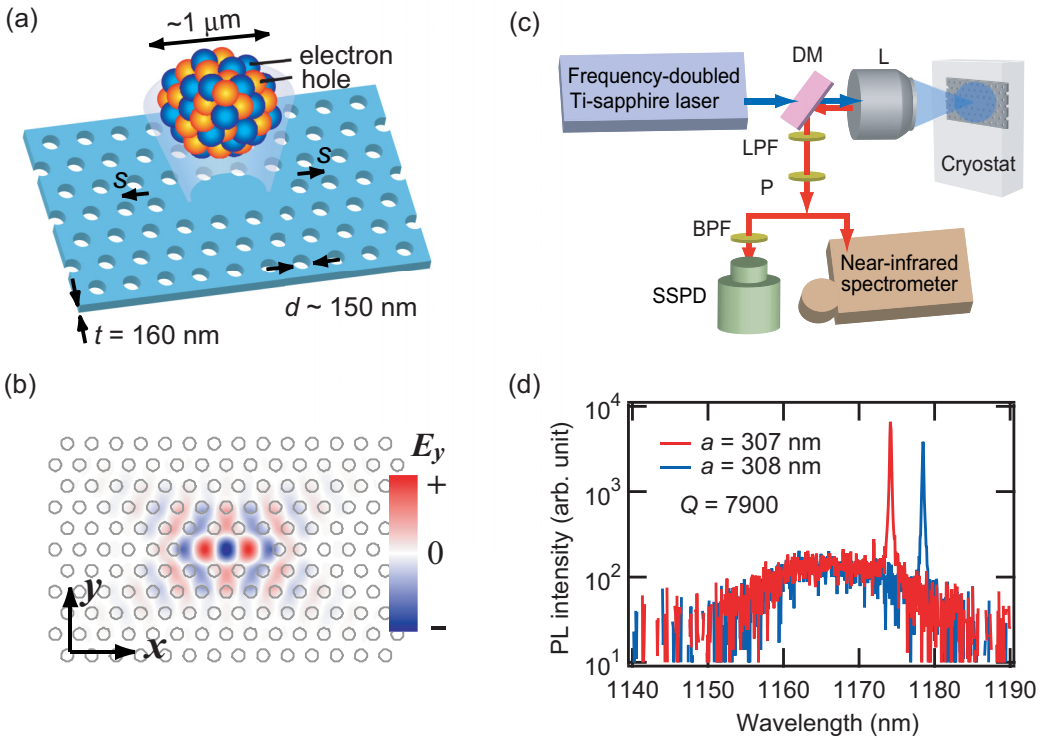

FIG. 1. (a) Dimensions of a fabricated $L3$ cavity with surface oxide and an EHD consisting of electrons and holes. The typical diameter of the EHD is comparable with a length of the $L3$ cavity. (b) Snapshot of the spatial distribution of a cavity-confined electric field directed towards the y axis (E_y). This mode is a fundamental cavity mode. (c) Setup for photoluminescence measurements. DM: dichroic mirror; L: objective; LPF: optical low-pass filter; P: polarizer; BPF: bandpass filter. (d) Typical PL spectra of the surface-oxidized Si PhC nanocavities with lattice periods of 307 and 308 nm and no end-hole shift. The spectral resolution is 0.1 nm and the sample temperature is 4 K.

cavity-enhanced SE rate of the Si EHD is still smaller than the nonradiative recombination rates of Si, where the EHD is uniformly annihilated inside and outside the nanocavities and at resonant and off-resonant wavelengths [21]. These EHD characteristics shown in later sections simplify the theoretical model for the Purcell effect of fast-dephasing emitters.

II. EXPERIMENT

Time-integrated and time-resolved photoluminescence measurements were performed to observe the EHD emission from Si PhC nanocavities. The Si PhC structures were fabricated in a 160-nm-thick Si membrane on a silicon-on-insulator wafer. The air hole was 150 nm in diameter. The lattice period of the PhC structure (a) was varied for each sample to change the resonant wavelength of the Si PhC nanocavity. To suppress the surface recombination of e-h pairs created in the Si PhC nanocavities, a 10-nm-thick oxide was formed over the entire Si PhC surface by thermally oxidizing the samples [21]. The optical cavity was formed by the three missing air holes in the PhC structure, which is called an $L3$ cavity. Figure 1(a) shows a schematic view of the fabricated Si PhC cavity. The air holes at both ends of the $L3$ cavity were shifted outwards to change the cavity Q value while leaving the mode volume unchanged. We performed a numerical simulation with the finite difference time domain (FDTD) method to estimate the cavity mode volume, and excitation and detection efficiencies for the emitters. Figure 1(b) shows the electric field distribution of the fundamental cavity mode. The optical field is confined around the $L3$ cavity. The sample was cooled to 4 K with a liquid helium flow cryostat as shown in Fig. 1(c). To create EHDs in Si PhC cavities, a pulsed ultraviolet laser light with a pulse width of 1 ps was focused on the center of an $L3$ cavity through an objective. The PL from the sample was collected by the objective and guided to a near-infrared spectrometer with a spectral resolution of 0.06 or 0.1 nm. The diameters of the excitation and detection spots were both approximately 3 μm. A time-resolved PL measurement was performed with a superconducting single-photon detector that had a timing resolution of 140 ps.

III. RESULTS

Figure 1(d) shows typical PL spectra of two Si PhC nanocavities with different lattice periods. In both cavities, a broadband spectrum was commonly detected at a wavelength of 1165 nm with a linewidth of 19 nm. In addition, we observed large narrowband spectral peaks that overlaid the broadband emission. The spectral peaks shifted by 4 nm when the lattice period was increased by 1 nm. We assigned the broadband PL to the SE of the EHD mediated with emissions of transverse and longitudinal optical (TO and LO) phonons, which agrees with the previously reported emission wavelength and linewidth [22]. These EHD emissions can be observed in thin Si membranes under a high concentration of e-h pairs created by an ultraviolet laser. The TO- and

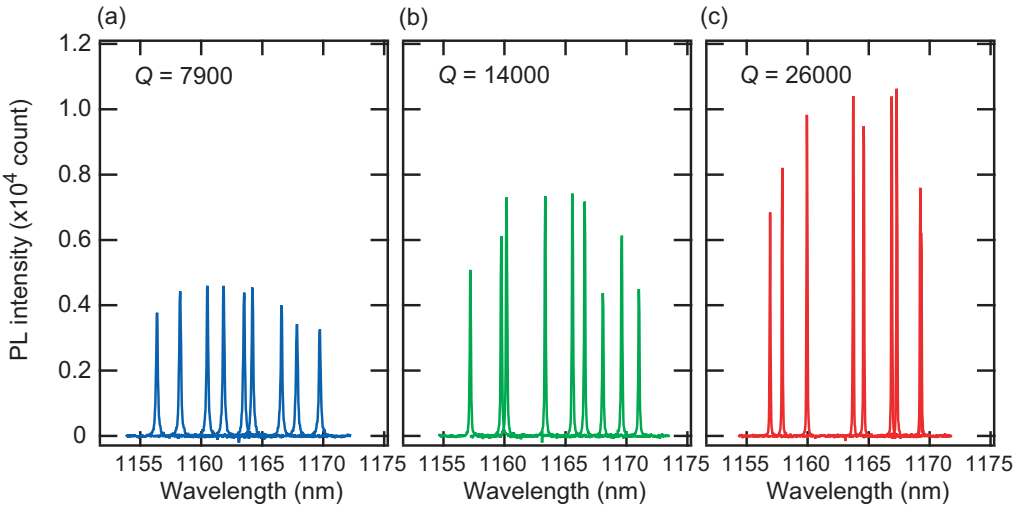

FIG. 2. Cavity-enhanced components of the PL spectra for Si PhC nanocavities with Q values of (a) 7900, (b) 14 000, and (c) 26 000. In each graph, the spectra of nanocavities with different lattice periods are overlaid. The spectral resolution is 0.06 nm. The average excitation laser power and repetition frequency are 30 μW and 8 MHz, respectively. The exposure time is 60 s.

LO-phonon emissions compensate the momentum mismatch of the e-h recombination between the valence band at the Γ point and the conduction band minimum near the X point in the indirect bandgap structure of Si. The large spectral peak that shifts when the PhC lattice period is changed is the EHD emission enhanced by the resonant PhC nanocavity. The cavity-enhanced emission is overlaid on the broadband EHD emission because the excitation and detection area defined by the objective is larger than the $L3$ PhC cavity. The objective detects the broadband emission from the EHD in the PhC structure surrounding the nanocavity although the cavity-enhanced narrowband emission originates only from the EHD that remains inside the nanocavity.

To extract the cavity-enhanced emission for discussion of the Purcell effect, the background EHD emission was subtracted from raw PL spectra. Figure 2 shows the cavity-enhanced components of the EHD emission in samples with three different end-hole shifts of the $L3$ cavity. Each graph shows the multiple spectra with different lattice periods ranging from 297 to 304 nm. These spectra were obtained by using a spectrometer with a high spectral resolution. The peak intensity of the cavity-enhanced PL is largest around 1165 nm, which agrees with the center wavelength of the broadband EHD emission shown in Fig. 1(d). The average cavity Q values (Q_{avg}) estimated from the linewidths of the spectral peaks are 7900, 14 000, and 26 000 for $s = 0$, $0.08a$, and $0.15a$, respectively. The cavity Q value is increased by increasing the shift of the end hole of the $L3$ cavity, which reduces the optical out-of-plane loss of the cavities [19]. A comparison of Figs. 2(a)–2(c) reveals that the peak intensities of the cavity-enhanced PLs increase gradually as the cavity Q value increases.

Figure 3 shows the time-resolved PL results for resonant cavities, which reveal the emission dynamics of the cavity-enhanced PL with different cavity Q values. Figure 3(a) also shows the PL decay of the EHD at off-resonance. The nonexponential decay at the end of the PL is caused by the thermal evaporation of the EHD [23]. No significant change is observed in the PL decay for any of the cavities while the cavity Q value varies. In addition, Fig. 3(a) indicates no change in the PL decay whether or not the EHD couples with the resonant cavity. The PL lifetimes of all the data are estimated to be 22 ns. The PL lifetime independent of both the cavity Q value and the resonance shows that the cavity-enhanced PL is not determined by the SE of the EHD, but by nonradiative

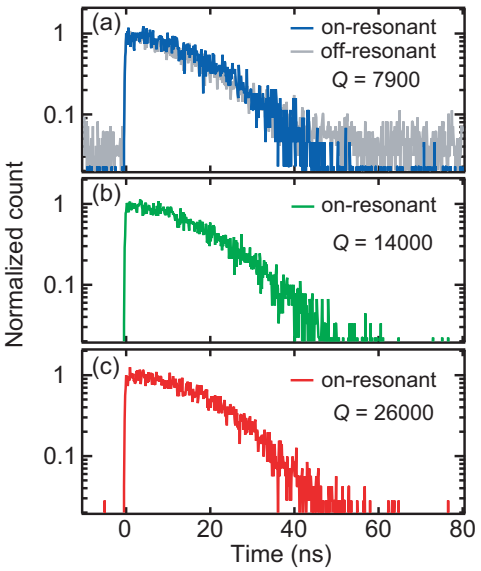

FIG. 3. Normalized PL decays for resonant PhC nanocavities with different Q values of (a) 7900, (b) 14 000, and (c) 26 000. The detection wavelengths of the resonant cavity are 1161, 1163, and 1162 nm for (a–c), respectively. The detection bandwidth is 1 nm. The graph for $Q = 7900$ shows the PL decay at a wavelength detuned by -2 nm from the cavity resonance. The PL lifetime is 22 ns, which is defined as the time it takes for the normalized PL intensity to reach e^{-1}. The data accumulation times for on- and off-resonant emissions are 120 and 3600 s, respectively. The average excitation laser power and repetition frequency are 30 μW and 8 MHz, respectively.

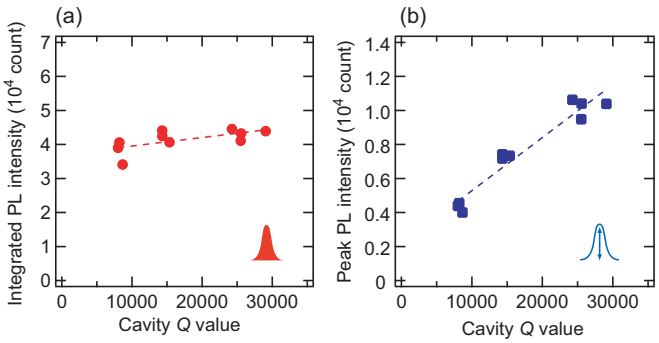

FIG. 4. (a) Integrated PL intensity and (b) peak PL intensity of the cavity-enhanced components of the EHD as a function of the cavity Q value. They are calculated from Fig. 2. The plotted data are taken at the spectral detuning of less than 5 nm between the cavity resonance and the center wavelength of the EHD emission (1165 nm). The broken lines are fitted to the data as a guide to the eye.

recombination because the PL lifetime ($\tau_{\rm PL}$) is described by $1/\tau_{\rm PL} = 1/\tau_{\rm SE} + 1/\tau_{nr}$, where $\tau_{\rm SE}$ and τ_{nr} are the SE and nonradiative recombination lifetimes, respectively. If the cavity-enhanced SE dominates the PL, the PL lifetime will be changed by the cavity resonance and the Q value due to the SE lifetime reduction by the Purcell effect. However, in our device, the cavity-enhanced SE lifetime of the EHD is still larger than the nonradiative recombination lifetime of surface and Auger recombination in Si PhC devices. When the PL decays are dominated by nonradiative recombinations, the PL intensities are experimental data necessary for quantitative discussion about the Purcell effect.

Figure 4 shows the integrated and peak intensities of the cavity-enhanced EHD emission as a function of the cavity Q value. The plotted data are taken at a spectral detuning ($\delta\lambda$) of less than 5 nm between the cavity resonance and the center wavelength of the intrinsic EHD emission. This threshold in the detuning is a quarter of the experimental PL linewidth of the EHD, which is estimated to be 19 nm from Fig. 1(d). As seen in Fig. 2, the PL intensities for a detuning larger than 5 nm tend to be smaller than that for smaller detuning, which might be attributed to the decoupling of the EHD emission centered at 1165 nm. All the PL intensity data are slightly scattered due to a fluctuation in the positional alignment of the objective adjusted to each cavity. In Fig. 4(a), the integrated intensity of the cavity-enhanced EHD emission increases slightly as the cavity Q increases, but is almost constant. In contrast, Fig. 4(b) clearly shows that the peak intensity is proportional to the cavity Q value.

IV. DISCUSSION

A theoretical discussion helps us to understand the cavity-Q dependence of experimentally obtained cavity-enhanced PL intensities of the EHD as shown in Fig. 4. In the discussion, emission dephasing should be considered because photon emitters, namely, e-h pairs consisting of EHDs, are exposed by various dephasing processes including scattering with phonons and charged particles. This study employs a semiclassical approach taking account of both the dephasing and spectral inhomogeneity of emitters.

First, we simulate the cavity-enhanced SE rate and PL intensities of a single emitter. Here, the temporal dephasing of the emission is introduced into the transition electric dipole moment of an e-h pair. The cavity-enhanced SE rate of a single emitter with dephasing is expressed by

$$\gamma_c(\omega_a,\boldsymbol{r}) = \int \frac{\xi(\boldsymbol{r})\pi\omega d_0}{\hbar n^2\varepsilon_0 V_c}\frac{\kappa/2\pi}{(\omega-\omega_c)^2+(\kappa/2)^2} \times \frac{\gamma_d/2\pi}{(\omega-\omega_a)^2+(\gamma_d/2)^2}d\omega, \quad (1)$$

where n, d_0,ω_a, and γ_d are the refractive index of the host material (3.45 for Si), the electric dipole moment strength of a radiative transition, the center frequency, and the dephasing rate of the emitter, respectively. For the cavity, ω_c and κ are the resonant frequency and the photon loss rate defined by ω_c/Q, respectively. The factor $\xi(\boldsymbol{r})$ is defined by $|\boldsymbol{E}(\boldsymbol{r})\cdot\boldsymbol{e}|^2/\max(|\boldsymbol{E}|^2)$, which means the electromagnetic coupling strength at the position of the emitter $\boldsymbol{r}$ between the optical electric field $\boldsymbol{E}$ confined in the cavity and the dipole oriented along a unit vector $\boldsymbol{e}$. The first and second terms in the integral indicate the SE rate enhanced by the cavity, and the last Lorentzian term expresses the dephasing of the emitter in the spectral domain. The intrinsic SE rate in a vacuum is given by $\gamma_0 = n\omega_a^3 d_0/(3\pi\varepsilon_0\hbar c^3)$, which is set at $5\,{\rm ms}^{-1}$, assuming that the SE rate of an e-h pair in an EHD is equal to that of an exciton in bulk Si [24].

On the assumption of perfect coupling $\xi(\boldsymbol{r}) = 1$ for simplicity, Fig. 5(a) shows the enhancement ratio of the SE rate γ_c/γ_0, which is called the Purcell factor, as a function of κ/γ_d. The cavity resonance is adjusted to the center frequency of the EHD emission where $\omega_c = \omega_a$. This figure also shows the Purcell factors calculated with different cavity V_c values for comparison while the V_c of the $L3$ PhC cavities is approximately $0.026\,\mu{\rm m}^3$. When $\kappa/\gamma_d \gg 1$, the SE rate enhancement increases linearly with increases in the cavity Q value, which is supported by $\gamma_c/\gamma_0 = 6\pi c^3 Q/(n^3\omega_c^3 V_c)$ derived from Eq. (1) in the region of $\kappa/\gamma_d \gg 1$. This dependence is well known in the Purcell effect, which was first proposed without considering the dephasing of the emitter [1]. However, when the dephasing rate or cavity Q value is increased, the Purcell factor does not exhibit a proportional relation and saturates at a certain value. In the region of $\kappa/\gamma_d \ll 1$, the Purcell factor is insensitive to the cavity Q, but depends strongly only on the cavity mode volume. Since the SE rate increases as a function of $1/V_c$ in the large γ_d region, the PhC and plasmonic devices with a smaller V_c are more suitable for the larger emission enhancement of fast-dephasing emitters [25–28].

Next, the integrated and peak intensities of the emission are simulated using Eq. (1). The spectrum of the dephasing single emitter is expressed by

$$s_c(\omega,\boldsymbol{r}) = \frac{1}{\gamma_{nr}+\gamma_c}\frac{\xi(\boldsymbol{r})\pi\omega d_0}{\hbar n^2\varepsilon_0 V_c}\frac{\kappa/2\pi}{(\omega-\omega_c)^2+(\kappa/2)^2} \times \frac{\gamma_d/2\pi}{(\omega-\omega_a)^2+(\gamma_d/2)^2}, \quad (2)$$

where γ_{nr} is the nonradiative recombination rate for the emitter, which is $45\,\mu{\rm s}^{-1}$ for the EHD shown in Fig. 3. The first

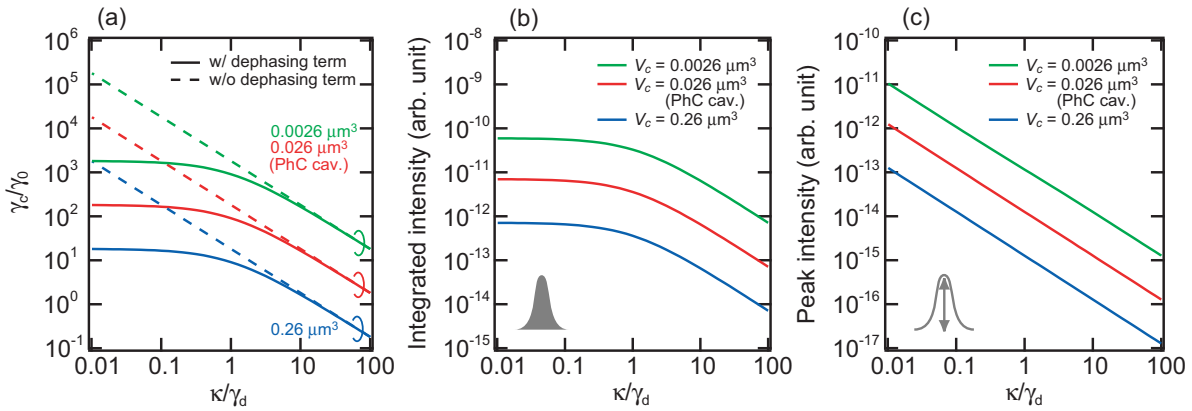

FIG. 5. (a) Calculated SE rate enhancement ratios with and without considering the dephasing of a single emitter as a function of κ/γ_d. (b) Integrated and (c) peak emission intensity of a cavity-enhanced single emitter calculated with the semiclassical model. Each graph shows the results calculated with different three mode volumes. The typical mode volume of the fabricated PhC nanocavities is around 0.026 μm^3.

and second terms mean the emission quantum efficiency (QE). The integrated and peak intensities are described by $\int s_c(\omega)\,d\omega$ and $s_c(\omega_c)$, respectively. They are shown in Figs. 5(b) and 5(c) when $\xi(\boldsymbol{r}) = 1$ and $\omega_c = \omega_a$. All the intensities are enhanced by the small V_c. The integrated intensity agrees well with the Purcell factor, which shows that the integrated intensity is an appropriate experimental measure for evaluating the Purcell effect. In the high-Q region, the integrated PL intensity is saturated because of the limit of the SE rate enhancement by the cavity. Here, the intensity saturation caused by a high QE ($\sim$1) that can be found when $\gamma_{nr} \ll \gamma_c$ is excluded from consideration. For the EHD, since $\gamma_{nr} \gg \gamma_c$ is satisfied even with a large γ_c in a cavity enhancement, QE $\ll 1$ where the QE is always proportional to the SE rate. This means that the SE rate enhancement by the resonant cavities increases the QE and achieves more efficient light emission. In contrast to the integrated PL intensity, the peak intensity is proportional to κ/γ_d over the entire range, which does not agree with the Purcell factor. The peak intensity increases as the cavity Q increases. This means that the emission energy of the dephasing single emitter is concentrated much more in the narrower linewidth of the cavity resonance under an almost constant integrated PL intensity.

Finally, the inhomogeneous spectral broadening of the emitter is taken into account in the calculation in order to simulate an actual EHD emission. Based on Eq. (2), the entire spectrum of an emission with inhomogeneous broadening is expressed by

$$\Sigma_c(\omega) = \eta_d \int d\omega_a \int d\boldsymbol{r} s_c(\omega,\omega_a,\boldsymbol{r}) N f(\omega_a). \qquad (3)$$

Here, $N = \eta_e I_p$ and $f(\omega_a)$ are the total number of e-h pairs consisting of the cavity-coupled EHD and the normalized Gaussian function expressing the inhomogeneous broadening, respectively. The inhomogeneous linewidth is set at 19 nm, which is estimated from the experimental PL linewidth of the EHD. I_p, η_e, and η_d are the pump rate, and the excitation and detection efficiencies for the objective, respectively. For each cavity, η_e and η_d, respectively, are estimated to be approximately 0.07 and 0.1 from an FDTD simulation [21]. The spectral and spatial hole burning induced by the cavity-enhanced SE is negligible because the PL decay is dominated by the nonradiative recombination even in a resonant cavity as shown in Fig. 3. The EHDs might be uniformly decayed in the spectral and spatial domains. The spatial integration in Eq. (3) is replaced by the constant $\sim$0.3, which includes the spatial and polarization coupling factors averaged for all the emitters in the cavity [6]. The simulated integrated intensity $\int \Sigma_c(\omega)d\omega$ is indicated in Fig. 6 as a function of the cavity Q with different dephasing times. The integrated intensity for an inhomogeneously broadened emitter exhibits the same feature as that for the single emitter shown in Fig. 5(b). When the cavity Q exceeds a critical value satisfying $\kappa/\gamma_d \ll 1$, the intensities are saturated. This figure also plots the experimental data shown in Fig. 4(a). In the cavity Q range covered by the experimental results, the integrated intensity becomes flatter as the dephasing time becomes smaller. If the dephasing time for an exciton in Si is assumed to be 1 ps, the integrated intensity calculated here is consistent with the experimental intensity as seen in Fig. 6. In this case, the Purcell factor (γ_c/γ_0) and the corresponding QE enhancement ratio are estimated to be $\sim$100 from Fig. 5(a) while the enhancement

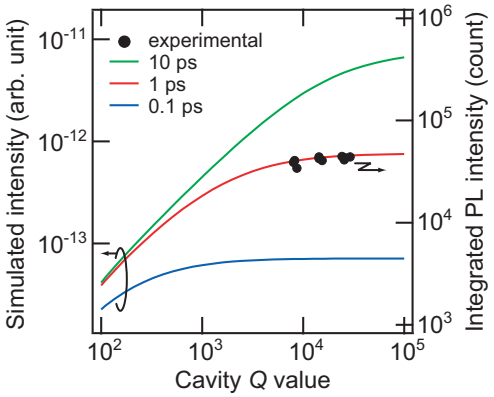

FIG. 6. Simulated intensities of the cavity-enhanced PLs with the inhomogeneous broadening and three different dephasing times. The experimental integrated PL intensities are also shown. The simulated data agree well with the experimental data assuming a dephasing time of 1 ps.

factors are saturated by the fast dephasing. The experimental dephasing time of EHDs has never been reported; however, the dephasing time assumed here is comparable with the pure dephasing time (T_2^*) of excitons in III-V semiconductors measured with the four-wave mixing method [29,30], where T_2^* is in the range from 1 to 10 ps due to the exciton-exciton and exciton-phonon scatterings. At the dephasing time of 1 ps, the PL intensity is almost constant until $Q \sim 1000$, but the intensity is proportionally decreased when the Q value is less than 1000. Recently, similar dependence has been observed in an InGaAsP-QWs island embedded in an InP PhC nanocavity, where the QWs island suppresses the exciton diffusion from the nanocavity [17]. The PL rate of the QWs is weakly saturated in a high Q value although there might be population redistributions of cavity-coupled excitons.

V. SUMMARY

This study described an EHD emission enhanced by Si PhC nanocavities with different Q values to discuss the Purcell effect of a fast-dephasing emitter. The use of an EHD enables us to exclude the outdiffusion, and spectral and spatial redistributions of *e-h* pairs coupled with PhC nanocavities. The experimental and theoretical results demonstrate that the cavity enhancement of the integrated PL intensity is saturated when the photon loss rate of the cavity is smaller than the dephasing rate, which coincides with the cavity-enhanced SE rate of a fast-dephasing emitter. This means that the integrated PL intensity is a key measure for estimating the SE rate enhancement even if the nonradiative decay dominates the observed PL decay of the emitter.

The theoretical results also show that a smaller cavity V_c induces a greater enhancement of the integrated PL intensity and the SE rate. This suggests that a plasmonic nanocavity with an ultrasmall V_c is preferable in terms of obtaining a greater emission enhancement with fast-dephasing emitters. However, some applications, for example, wavelength division multiplexing, need narrowband emissions. Since plasmonic nanocavities typically have Q values less than 100 due to the optical loss in metals, high-Q PhC nanocavities are more suitable for obtaining intense narrowband emission. The PhC nanocavity concentrates the emission energy of the fast-dephasing emitter in high-Q cavity resonances thanks to PL enhancement by the resonant cavity. This study constitutes a guide to the large emission enhancement of fast-dephasing emitters such as excitons in bulk and QWs of semiconductors, and will contribute to the development of bright narrowband light emitting devices based on PhC and plasmonic nanocavities.

ACKNOWLEDGMENTS

We thank Dr. K. Nishiguchi for performing the sample oxidation and Dr. T. Tamamura and D. Takagi for their help with sample fabrication. This work was part of a research project supported by the National Institute of Information and Communications Technology (Grant No. NICT-QAT113u02) in Japan.

[1] E. M. Purcell, Phys. Rev. **69**, 681 (1946).
[2] S. Noda, M. Fujita, and T. Asano, Nat. Photonics **1**, 449 (2007).
[3] M. S. Tame, K. R. McEnery, S. K. Özdemir, J. Lee, S. A. Maier, and M. S. Kim, Nat. Phys. **9**, 329 (2013).
[4] D. J. Heinzen, J. J. Childs, J. E. Thomas, and M. S. Feld, Phys. Rev. Lett. **58**, 1320 (1987).
[5] P. Borri, W. Langbein, S. Schneider, U. Woggon, R. L. Sellin, D. Ouyang, and D. Bimberg, Phys. Rev. Lett. **87**, 157401 (2001).
[6] H. Sumikura, E. Kuramochi, H. Taniyama, and M. Notomi, Sci. Rep. **4**, 5040 (2014).
[7] A. Faraon, C. Santori, Z. Huang, V. M. Acosta, and R. G. Beausoleil, Phys Rev. Lett. **109**, 033604 (2012).
[8] K. Seeger, *Semiconductor Physics. An Introduction* (Springer-Verlag, Berlin, 2004).
[9] M. P. van Exter, G. Nienhuis, and J. P. Woerdman, Phys. Rev. A **54**, 3553 (1996).
[10] Y. Xu, R. K. Lee, and A. Yariv, Phys. Rev. A **61**, 033807 (2000).
[11] H. Y. Ryu and M. Notomi, Opt. Lett. **28**, 2390 (2003).
[12] A. Auffèves, B. Besga, J.-M. Gérard, and J.-P. Poizat, Phys. Rev. A **77**, 063833 (2008).
[13] A. Naesby, T. Suhr, P. T. Kristensen, and J. Mørk, Phys. Rev. A **78**, 045802 (2008).
[14] S. Iwamoto, Y. Arakawa, and A. Gomyo, Appl. Phys. Lett. **91**, 211104 (2007).
[15] M. Fujita, Y. Tanaka, and S. Noda, IEEE J. Sel. Top. Quantum Electron. **14**, 1090 (2008).
[16] T. Baba, D. Sano, K. Nozaki, K. Inoshita, Y. Kuroki, and F. Koyama, Appl. Phys. Lett. **85**, 3989 (2004).
[17] M. Takiguchi, H. Sumikura, M. D. Birowosuto, E. Kuramochi, T. Sato, K. Takeda, S. Matsuo, and M. Notomi, Appl. Phys. Lett. **103**, 091113 (2013).
[18] I. Fushman, D. Englund, and J. Vučković, Appl. Phys. Lett. **87**, 241102 (2005).
[19] Y. Akahane, T. Asano, B.-S. Song, and S. Noda, Nature **425**, 944 (2003).
[20] M. Capizzi, M. Voos, C. Benoit à la Guillaume, and J. C. McGroddy, Solid State Commun. **16**, 709 (1975).
[21] H. Sumikura, E. Kuramochi, H. Taniyama, and M. Notomi, Opt. Express **24**, 1072 (2016).
[22] M. Tajima and S. Ibuka, J. Appl. Phys. **84**, 2224 (1998).
[23] C. D. Jeffries, Science **189**, 955 (1975).
[24] J. D. Cuthbert, Phys. Rev. B **1**, 1552 (1970).
[25] S. Nakayama, S. Ishida, S. Iwamoto, and Y. Arakawa, Appl. Phys. Lett. **98**, 171102 (2011).
[26] K. J. Russell, T.-L. Liu, S. Cui, and E. L. Hu, Nat. Photonics **6**, 459 (2012).
[27] G. M. Akselrod, C. Argyropoulos, T. B. Hoang, C. Ciracì, C. Fang, J. Huang, D. R. Smith, and M. H. Mikkelsen, Nat. Photonics **8**, 835 (2014).
[28] N. P. de Leon, B. J. Shields, C. L. Yu, D. E. Englund, A. V. Akimov, M. D. Lukin, and H. Park, Phys Rev. Lett. **108**, 226803 (2012).
[29] L. Schultheis, J. Kuhl, A. Honold, and C. W. Tu, Phys. Rev. Lett. **57**, 1635 (1986).
[30] H. J. Bakker, K. Leo, J. Shah, and K. Köhler, Phys. Rev. B **49**, 8249 (1994).